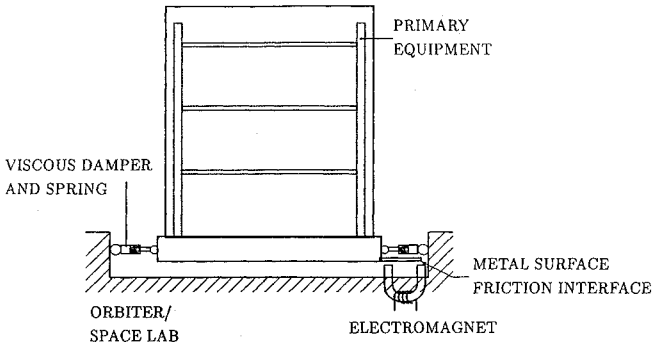

Fig. 1a Schematic diagram of equipment with the AFC system.

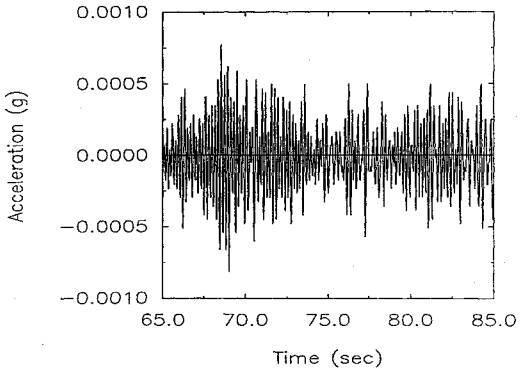

Fig. 1b Time history of the STS-40 x-axis orbital acceleration.

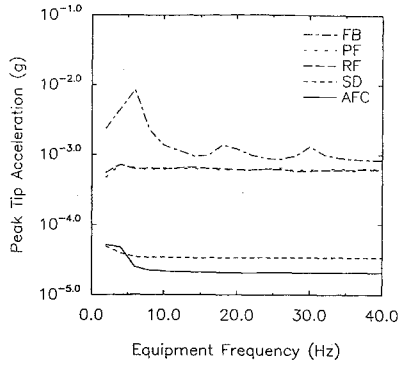

Fig. 2 Equipment peak response for the fixed-base and vibration control mechanisms due to orbital excitation.

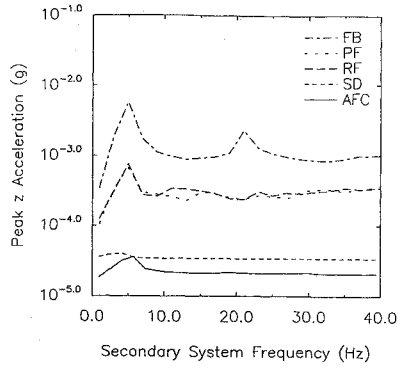

Fig. 3 Secondary system peak response for the fixed-base and vibration control mechanisms due to orbital excitation.

control systems, the transitions from the sliding to the nonsliding phase generate shock loadings and lead to the excitation of the higher harmonics. Therefore, five vibration modes of the equipment are used in the analysis in order to best model the response during this transition.

Figure 2 shows the peak acceleration of the tip of the equipment as a function of the equipment frequency. The fixed-base response is used as a baseline for comparison. The responses of the passive friction-based system are of the same order of magnitude as those of the fixed-base system, because of the slip–stick shock loadings. The SD system, which is the most effective among the passive systems considered, provides an order-of-magnitude decrease in peak responses with respect to the baseline. Figure 2 shows that the AFC system leads to the lowest peak responses.

Peak subsystem responses to orbital excitation are shown in Fig. 3. The response spectra in this figure are plotted versus subsystem frequency. A value of 35 Hz was used for the equipment frequency. The graphs show that the passive friction control systems lead to subsystem responses that are of the same order as the baseline. Other passive control mechanisms provide some isolation from the orbital excitations. The AFC mechanism appears to be the most effective system in reducing the peak responses experienced by the subsystem.

Conclusions

A numerical simulation was performed using a shear beam to represent equipment in a space laboratory. Several vibration control mechanisms, including three passive and one active system, were evaluated. Based on the presented results, the following conclusions are drawn. Use of passive and active vibration control mechanisms reduces the peak accelerations experienced by the equipment and its subsystem in the orbital environment. The active friction control mechanism considered provides the best performance in reducing the peak acceleration transmitted to the equipment and its subsystem. With the use of the AFC mechanism, the peak orbital acceleration experienced by the equipment was reduced to about $20 \times 10^{-6} g$.

Acknowledgments

This work is supported by the NASA Lewis Research Center, Cleveland, Ohio, under Grant No. NGT-50825.

References

[1]Grodsinsky, C. M., "Development and Approach to Low-Frequency Microgravity Isolation Systems," NASA TP-2984, 1990.

[2]Srinivasan, A. V., "Dynamic Friction," *Proceedings of the Symposium on Large Space Structures: Dynamics and Control*, (May 1988), Vol. 1, pp. 174–194.

[3]Ellison, J. F., Ahmadi, G., and Grodsinsky, C., "Microgravity Vibration Control Using Passive and Active Mechanisms," Rept. MAE-258, Clarkson Univ., Potsdam, NY, Sept. 1992.

[4]Su, L., Ahmadi, G., and Tadjbakhsh, I. G., "A Comparative Study of Base Isolation Systems," *Journal of the Engineering Mechanics Division, ASCE*, Vol. 115, No. 9, 1989, pp. 1976–1992.

[5]Ahmadi, G., and Su, L., "Equipment Response Spectra for Base-Isolated Shear Beam Structures," *Nuclear Engineering and Design*, Vol. 132, No. 3, 1992, pp. 287–308.

[6]Lee-Glauser, G., and Ahmadi, G., "Dynamic Response Spectra for an Aerospace Payload and Its Attachments," Rept. MIE-232, Clarkson Univ., Potsdam, NY, May 1991.

A. L. Vampola
Associate Editor

Reusable Sounding-Rocket Design

Dick L. Y. Woo* and James A. Martin†
University of Alabama,
Tuscaloosa, Alabama 35487-0280

Introduction

IN an era of reduced budgets and project cost cutting, the ideas of reusability and cost-effectiveness in launch vehicles have become highly important. Although these ideas have had some success with

Received June 7, 1994; revision received Oct. 21, 1994; accepted for publication Nov. 19, 1994.

*Undergraduate Student, Aerospace Engineering. Member AIAA.

†Associate Professor, Aerospace Engineering. Associate Fellow AIAA.

the Space Shuttle, the primary goals of cheaper and more frequent flights have not been realized. One particular class of rockets that may be more suitable is sounding rockets. These vehicles operate in a less demanding environment, and there is potential for many more flights. By augmenting the basic rocket configuration with wings, landing gear, flight controls, and guidance systems, the flight vehicle now has the ability to glide and land back at the launch site or at a specific recovery site. A design of such a reusable rocket is presented. The design presented is not likely to be useful for many sounding-rocket missions, but it is intended to prove the economies of a reusable rocket vehicle. Concerns such as the ground turnaround time and costs could be examined.

General Configuration and Layout

The basic configuration of the flight vehicle is shown in Fig. 1. The most obvious design characteristic is the pivoting wing on the top of the fuselage. The wing is deployed during the descent for the glide back to earth. The placement of the various systems are illustrated in Fig. 2. Other significant design features are summarized in Table 1.

Engine

The design of the reusable sounding rocket is based on the LR101-NA-7 venier engine.[1] This engine is one of the components in the MA-3 propulsion system used on the Atlas rocket. The choice of this engine was made as a result of an agreement by the manufacturer to provide an engine if funding for a cooperative effort were secured for construction of a reusable rocket.

Table 1 Summary of design characteristics

Gross liftoff weight	553 lb
Burnout weight	353 lb
RP-1 weight	71 lb
Liquid-O_2 weight	129 lb
Thrust, sea level	830 lb
Thrust-to-weight ratio	1.5
Airfoil section	NACA 4415
Wing aspect ratio	6.2
Fuselage length	21 ft
Static margin	19%
Maximum L/D	12.8
Speed at max. L/D	62 knots
Landing speed	52 knots

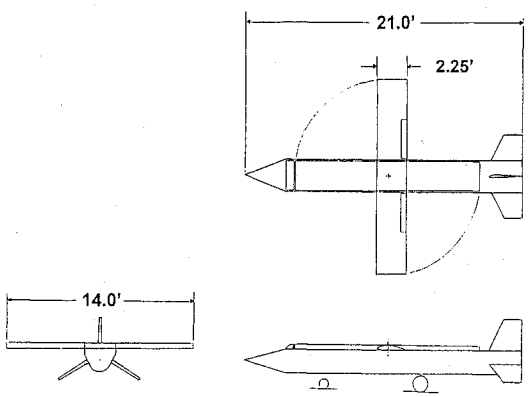

Fig. 1 General configuration.

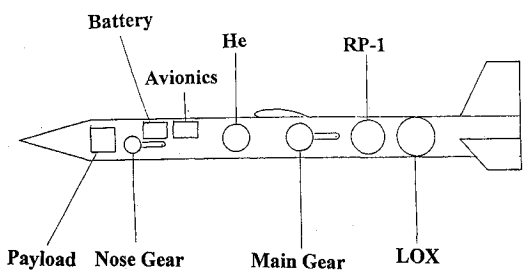

Fig. 2 System layout.

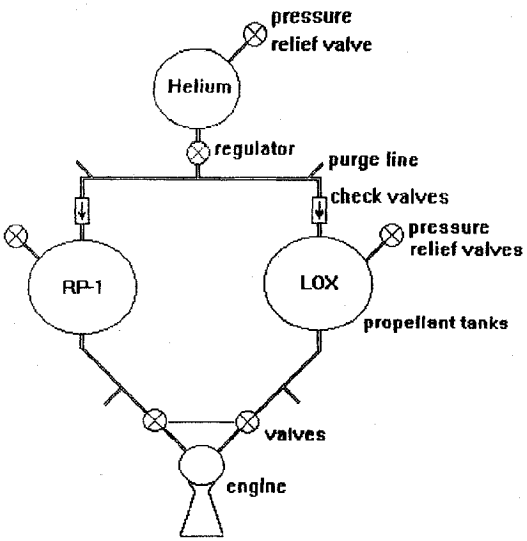

Fig. 3 Propellant feed system.

To minimize the complexity of the engine and associated systems, two simplifications were made. First, the gimbaling capability of the stock engine will not be used, which eliminates the need for the hydraulics required to drive the mechanism. It also keeps weight to a minimum.

The second simplification involves the feed system. Instead of utilizing pumps to deliver the RP-1 fuel and liquid oxygen to the engine, a pressure-fed system is used. This system consists of a high-pressure tank for the pressurizing medium, in this case helium, and a regulator to maintain constant pressure, ensuring fairly constant propellant flow rates. The tank is pressurized initially to 5000 psia, and the regulator maintains the line pressure at 550 psia. This high-pressure tank is of a filament-wound design, weighing 15 lb, less than half the weight of a comparable spherical steel tank. The feed system is shown in Fig. 3.

Wing

A pivoting wing design was chosen to minimize drag during the ascent phase of the launch. The wing is stowed adjacent to the fuselage during launch and is deployed mechanically following the trajectory apogee.

The wing pivot system consists of a rotating shaft (to which the wing is mounted), a rotational spring, and a dashpot. Rotating the wing to the stowed position places the spring in tension. The spring can now provide the force required to move the wing to the deployed position for the glide back to earth. The dashpot slows the shaft rotation as the wing approaches its final position and reduces the impact loads as the wing reaches the wing stop.

The use of a rotational spring allows the deployment of the wing to be rapid. This feature is beneficial in the event of a premature shutdown of the engine during the ascent. Quick deployment of the wing is essential for the recovery of the vehicle in this condition.

Fuselage

The size and shape of the fuselage was dictated by the wing. The cross section is generally triangular in shape, with one flat surface used for the wing stowage. This shape creates a large and wide fuselage, allowing for structurally efficient spherical propellant tanks to be used. Opposite the flat surface, the fuselage is more rounded to conform to the spherical tanks.

The three fins at the rear of the vehicle perform a dual role. The fins are initially locked in place, and act as stabilizing fins for the rocket during its ascent. They are also all-moving tail surfaces, and provide pitch and directional control during the glide to the recovery site.

Automatic Control and Navigation

Control of the vehicle is to be automated during the majority of the descent. This phase begins following wing deployment and continues until the start of the landing cycle. The landing sequence will be accomplished through remote control by a ground controller at the recovery site.

Because the vehicle cannot be sighted visually during the initial portion of the descent, it must be flown automatically. A three-axis autopilot will be employed to maintain the proper vehicle attitude. Only when the vehicle has come within sight of the recovery area will it be released to manual control.

The vehicle will be equipped with a long-range navigation system (LORAN), which will be coupled directly to the autopilot. Prior to launch, waypoints are programmed into the LORAN. When the autopilot is activated, the vehicle files a specific descent profile.

Electrical System

An eight-channel receiver is used to control the functions of the flight vehicle. Of the eight channels, four are assigned to the autopilot and primary flight controls. Servomechanisms are used as the actuating mechanisms. During autopilot operation the three primary flight control channels (elevator, rudder, and ailerons) from the receiver are disabled, allowing signals from only the autopilot to activate the servomechanisms. Conversely, when the autopilot is disengaged, the three flight control channels are active. This approach allows only one set of signals to reach the flight controls, either from the autopilot or from the ground controller.

The remaining four channels are assigned to engine start, wing lock release, landing-gear release, and flaps. At the instant of engine start, a timer is activated, and the wing lock is released at a predetermined elapsed time. This serves as a backup feature, allowing wing deployment to occur in the event that no signals are received from the ground controller.

Trajectory Analysis

An analysis of the trajectory was conducted with SORT.[2] This program allows three-dimensional trajectory optimization. Only point-mass trajectories were analyzed. Engine burnout occurs 36 s after liftoff, at an altitude of 12,965 ft. The maximum altitude achieved by the vehicle is 18,870 ft.

Concluding Remarks

This paper indicates that it may be possible to design a simple reusable rocket. The next step will be to build and test such a vehicle. This design could be extended and adapted to larger vehicles in order to attain the higher altitudes that are required in some of the applications of sounding rockets, such as upper-atmospheric experiments.

Acknowledgments

The authors of the design report on which this Note is based deserve the credit for this design. They were the undergraduate design class of the Department of Aerospace Engineering of the University of Alabama in the spring of 1994. The members of the class were James Daniel, Kimberly Kunzweiler, Kazuhiro Nishita, TongSay Vongpaseuth, Bryan Warren, Juan Webb, and Dick Woo.

References

[1]Anon., "Technical Manual, LR101-NA-7," Rockwell International, Rocketdyne Division, Report R-6795-3, Canoga Park, CA, July 1987.

[2]Berning, M. J., and Frick, J. D., "User's Guide for the Simulation and Optimization of Rocket Trajectories (SORT) Program," Lockheed Engineering and Sciences Co., July 1989.

I. E. Vas
Associate Editor

Spacecraft Optimization with Combined Chemical–Electric Propulsion

Craig A. Kluever*
University of Missouri–Columbia/Kansas City, Kansas City, Missouri 64110

Introduction

RECENT research has involved vehicle and mission optimization for electric orbit transfer vehicles,[1–3] and lunar missions have been of specific interest.[4,5] Lunar missions using advanced all-chemical propulsion systems have also been investigated.[6] In this note, vehicle and trajectory optimization of a lunar–interplanetary mission using a combined chemical and electric propulsion system is performed. The mission scenario involves a translunar injection (TLI) from low Earth orbit (LEO) via the upper stage of a Delta II launch vehicle, followed by a lunar orbit insertion (LOI) chemical burn into an intermediate, high-altitude circular lunar orbit, followed by a low-thrust orbit transfer to a polar, circular low lunar orbit (LLO) using electric propulsion. After data are collected at the desired 100-km polar LLO (for instance, lunar gravity mapping), the spacecraft escapes the moon's gravity field using electric propulsion to initiate the interplanetary leg of the two-phase scientific mission. An explicit interplanetary target is not defined, so that the mission analysis can remain general yet at the same time retain the essence of a dual-mission scenario.

The optimization problem involves maximizing the spacecraft's payload for a given fixed launch-vehicle capability and fixed transfer time. The vehicle sizing feature requires computing the optimal chemical burns for TLI and LOI, the optimal electric input power P, and the optimal specific impulse I_{sp} for the electric propulsion stage. The mission design feature involves computing the optimal TLI conditions at LEO and the optimal lunar altitude and inclination for the LOI burn. The latter mission design feature defines how much of the transfer to polar LLO is performed by the chemical and by the electric propulsion stage. The vehicle and mission optimization features exhibit a strong interaction.

Payload and Propulsion-System Analysis

The total mass of a spacecraft with chemical and electric stages after TLI is

$$m_{TLI} = m_{p_c} + m_{dry_c} + m_{p_e} + m_{tank_e} + m_{pp} + m_{net} \qquad (1)$$

where m_p is the propellant mass, m_{dry_c} is the dry mass of the chemical stage, m_{tank_e} is the tank mass of the electric stage, m_{pp} is the power- and propulsion-system mass of the electric stage, and m_{net} is the net mass. The subscripts c and e represent the chemical and electric propulsion stages, respectively. The injected mass m_{TLI} is computed from a linear approximation of the launch performance of a Delta II vehicle[7]:

$$m_{TLI} = -27C_3 + 1227 \text{ kg} \qquad (2)$$

where C_3 is the injection energy (km^2/s^2). The propellant masses m_{p_c} and m_{p_e} are calculated from the rocket equation using the appropriate velocity change ΔV and I_{sp} for the respective maneuver. The specific impulse I_{sp} of the chemical stage is fixed at 310 s. The dry mass m_{dry_c} includes the structural, engine, and tank mass of the chemical stage and is assumed to be 15% of the chemical propellant mass.[6]

Received Sept. 19, 1994; revision received Jan. 12, 1995; accepted for publication Jan. 12, 1995.

*Assistant Professor, Mechanical and Aerospace Engineering Department. Member AIAA.